Post-print: Submitted, accepted an published in Journalof Physical Chemistry C 117 (42), 21735-21742 (2013); DOI: dx.doi.org/10.1021/jp4039804 |

Methanol Oxidation at Diamond-Supported Pt Nanoparticles: Effect of the Diamond Surface Termination

V. Celorrio,[†,‡] D. Plana,[†] J. Flórez-Montaño,[§] M.G. Montes de Oca,[†] A. Moore,[†] M.J. Lázaro,[‡] E. Pastor,[§*] and D.J. Fermín[†*]

[†] School of Chemistry, University of Bristol, Cantocks Close, Bristol, BS8 1TS, UK.

[‡] Instituto de Carboquímica (CSIC), Miguel Luesma Castán 4, 50018 Zaragoza, Spain.

[§]Universidad de La Laguna, Dpto. de Química-Física, Avda. Astrofísico Francisco Sánchez s/n, 38071 La Laguna (Tenerife), Spain.

* Corresponding author:

Dr David J. Fermín

Tel.: +44 117 9288981

E-mail address: David.Fermin@bristol.ac.uk

Dr Elena Pastor

Tel.: +34 922 318028; Fax: +34 922 318033

E-mail address: epastor@ull.es

ABSTRACT

The electrocatalytic reactivity of Pt nanoparticles supported on high-pressure-high-temperature diamond particles towards adsorbed CO, methanol and formic acid oxidation is investigated employing differential electrochemical mass spectrometry (DEMS). Surface treatment of diamond particles, employed as dimensionally stable electrocatalyst supports, leads to materials with surfaces featuring mainly hydrogen (HDP) or oxygen-based functional groups (ODP). Pt nanoparticles with average diameter below 5 nm were generated by impregnation of the modified diamond particles. The voltammetric responses associated with the oxidation of adsorbed CO appeared unaffected by the surface termination of the diamond support. However, significant differences were observed for methanol oxidation in acid solutions, with Pt/HDP producing smaller current densities than Pt/ODP and a commercially available Pt catalyst (Pt/E-TEK). DEMS studies show higher conversion efficiencies to CO_2 for Pt/ODP and Pt/E-TEK, while Pt/HDP exhibited values of approximately 90%. Evidence of formic acid generation as intermediate during methanol oxidation was obtained on all catalysts. Significant differences in the current density associated with the oxidation of formic acid were also observed, with Pt/HDP also providing the lowest current densities. The ensemble of the experimental data suggests that adsorbed $HCOO_{ads}$ species is the key intermediate in methanol oxidation, and its subsequent oxidation to CO_2 is strongly affected by the average surface termination of the diamond support.

1. INTRODUCTION

The electrocatalytic oxidation of methanol on Pt-based catalysts is one of the most studied reactions in the field of electrochemical energy conversion, yet mechanistic aspects remain controversial.[1-3] This multi-electron transfer reaction proceeds via a complex mechanism involving several parallel and consecutive pathways. As illustrated in **scheme 1**, methanol oxidation to CO_2 can take place via the generation of adsorbed CO, as well as reactive intermediates such as HCHO and HCOOH.[4-7] The reaction pathway can be affected by the structure and size of the Pt nanostructure, but also by the nature of the catalyst support, typically mesoporous sp_2 hybridized carbon.[8-11]

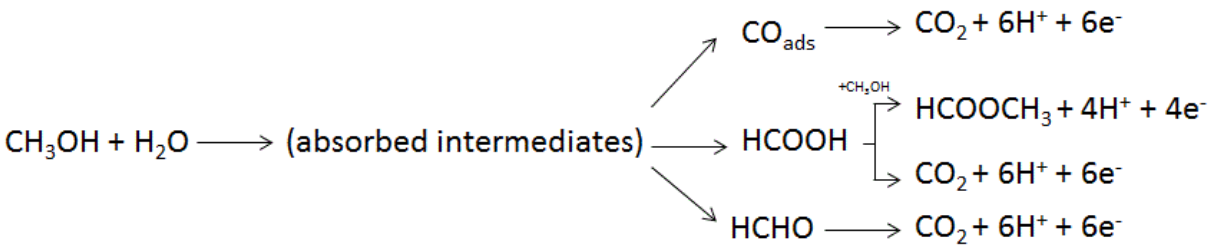

Scheme 1. Proposed mechanisms for methanol electro-oxidation at Pt surfaces.

The impregnation of metal precursors into carbon suspensions, followed by chemical reduction, is a widely used approach for generating nanoscale supported electrocatalysts. The properties of the carbon support can strongly influence key aspects of the metal nanocatalysts, such as mean size, morphology, size distribution, stability, dispersion and reactivity.[12-13] For instance, oxygenated functional groups have been shown to improve the wettability of carbon materials, enhancing both the interaction of the carbon with the metal precursor complexes and the anchoring of the metallic nanostructures.[14-15] Oxygenated groups can be introduced at the surface of mesoporous carbon by a variety of gas and liquid phase pre-treatments.[16-19] However, while introducing oxygen surface groups, other properties such as pore structure or specific surface area are inevitably affected. Consequently, the establishment of relationships between carbon surface termination and the reactivity of the supported catalysts is an extremely challenging issue. In a recent

work, the effect of various carbon pretreatments on the electrocatalytic activity of Pd nanostructures exhibited contrasting trends in the case of conventional impregnation versus incorporation of already prepared colloidal nanoparticles.[20]

An interesting alternative for electrocatalyst support involves diamond powders, which are characterized by a high chemical and mechanical stability, as well as a rich surface chemistry.[21] Depending on the preparation method, the surface of diamond powders can be H-terminated and/or feature a range of functional groups,[22-26] Moore et al. demonstrated that Pd nanostructures generated by impregnation on commercially available high-pressure-high-temperature (HPHT) diamond particles can be used as high surface area electrocatalysts for formic acid oxidation.[27] This approach is inspired by seminal studies on boron doped diamond (BDD) films, demonstrating their suitability as dimensionaly stable support for electrodeposited metal nanostructures.[28-30] Cabrera and co-workers investigated the performance of detonated diamond nanoparticles and boron-doped diamond powders, obtained by ion implantation, as a supports for Pt and PtRu catalysts in direct methanol fuel cells.[31-33] One of the key challenges in the implementation of non-boron doped diamond powders as electrocatalyst supports is their high bulk resistivity. However, charge transport in metal-diamond composites can be manipulated by the generation of percolation pathways,[34] "transfer-doping" mechanism in aqueous solution,[34-37] and via surface states and functional redox groups.[38-40]

In the present work, the reactivity of Pt nanostructures supported on high-pressure-high-temperature diamond powders is evaluated for the first time as a function of the effective surface diamond termination. Pt nanostructures were reduced at the surface of hydrogen (HDP) and oxygen terminated diamond powders (OPD) through impregnation methods. The electrocatalytic activity of these composites towards the oxidation of CO, methanol and formic acid were evaluated in acid solution employing differential electrochemical mass spectrometry (DEMS). Although the mean Pt particle size in Pt/HDP is slightly smaller than in Pt/ODP, the potential for oxidation of adsorbed CO is rather similar in both cases. Interestingly, the oxidation of CO_{ads} on the diamond supported Pt nanoparticles was characterized by a broad voltammetric peak centered at potentials 100 mV more

negative than on a commercially available Pt electrocatalyst (Pt/E-Tek); the latter is used as benchmark in this work. On the other hand, electrochemical data showed a significant difference in the reactivity of Pt/HDP and Pt/ODP with respect to methanol oxidation. DEMS measurements provided evidence that formic acid is generated during the oxidation of methanol. We finally concluded that the contrast in the reactivity of Pt/HDP and Pt/ODP mainly arises from differences in the oxidation kinetics of $HCOO_{ads}$ species generated as intermediate during methanol oxidation.

2. EXPERIMENTAL

2.1. Diamond surface termination. High-pressure-high-temperature diamond particles (type Ib), with a nominal size of 500 nm, were purchased from Microdiamant AG, Switzerland (MYS005). The as-received particles were initially washed by sonication in ultrapure water; O- and H-terminations were then generated following a previously described procedure.[36] Briefly, oxygenated surface groups are generated by heating the particles in a concentrated 9:1 v/v H_2SO_4:HNO_3 solution; the particles are then successively washed with Milli-Q water and centrifuged until the supernatant is pH neutral. Hydrogenation of the oxygen terminated particles is achieved by an 800 W microwave plasma reactor, at a pressure of 50 Torr, with a hydrogen flow rate of 500 sccm. Particles were allowed to cool down in the presence of hydrogen to approximately 250ºC, and under Ar to room temperature, before exposure to air. Changes of the surface termination of these diamond powders following these pre-treatments have been monitored by FTIR.[36] The specific surface area of the diamond particles, as estimated from BET analsys (results not shown) is 10.7 m^2 g^{-1}. Although higher specific surface areas could be obtained from smaller diamond particles, such as those obtained by detonation, these materials offer key advantages such as high crystallinity, low density of aggregates and low content of sp^2 impurities.

2.2. Electrocatalyst preparation. Electrocatalysts were prepared by the solution-reduction method, using sodium borohydride as reducing agent. 35 ml of 1.13 mM H_2PtCl_6 (Sigma-Aldrich) were added to 80 ml of an aqueous suspension of the diamond powder. The suspension was kept under

strong stirring for 24 hours, before the slow addition of 20 ml of 26.4 mM sodium borohydride, at room temperature.[8]

2.3. Differential electrochemical mass spectrometer experiments (DEMS). These experiments were carried out in the differential electrochemical mass spectrometer set-up described by Pérez-Rodriguez.[41] Briefly, the configuration used to perform DEMS experiments consisted in an electrochemical cell coupled to a Pfeiffer-Vacuum mass spectrometer, which contains a Prism QMS 200 detector, allowing acquisition up to 72 simultaneous mass/charge (m/z) signals.

A 50 cm^3 capacity plexiglass cell was used, with a hydrophobic Teflon membrane (Scimat Ltd., 200/40/60) at the bottom, which worked as an interface between the electrochemical cell and the mass spectrometer, being permeable to gaseous and/or volatiles products generated during the electrochemical reaction. The working electrode was placed between the Teflon membrane and a glassy carbon rod, which served as electrical contact.

Gas diffusion electrodes were used as working electrodes (7 mm diameter) prepared as reported elsewhere.[42] A carbon cloth was painted using the so called gas diffusion ink, composed by Vulcan XC-72R, ultrapure water (Millipore Milli-Q system), isopropanol (Merck, p.a.) and a PTFE dispersion (60 wt. %, Dyneon); resulting in a 20 wt.% PTFE mixture. This ink was painted onto one side of a carbon cloth, followed by heating at 320 °C for 1 h. Electrodes were made by depositing a suspension of Nafion solution (5 wt.%, Sigma-Aldrich) and the synthesized electrocatalyst on pieces of the pretreated carbon cloth. The final amount of metal active phase in all the prepared electrodes was approximately 0.4 mg_{Pt} cm^{-2}.

2.4. Characterization of the nanostructures and electrochemical studies. The structure and composition of the catalysts was investigated employing a suite of scanning electron microscopes: JEOL SEM 5600 LV, JEOL FEG-SEM 6330 and Hitachi S-3400 N fitted with an energy dispersive X-ray analyzer (EDX) Röntec XFlash Si(Li). X-ray diffraction (XRD) patterns were recorded using a Bruker AXS D8 Advance diffractometer with a θ-θ configuration and using CuKα radiation (λ = 0.154 nm). Scans were done for 2θ values between 0º and 100º. Scherrer's equation and Vegard's

law were applied to the (220) peak of the Pt fcc structure, around $2\theta = 70^{o}$, in order to estimate the Pt crystallite size and lattice parameters, respectively.

The electro-oxidation of adsorbed CO and methanol were investigated in the set up described in section 2.3, using a two-compartment electrochemical cell featuring a carbon rod and a reversible hydrogen electrode (RHE) as counter an reference electrodes. Argon (N50) was used to deoxygenate all solutions and CO (N47) was employed for the adsorption experiments. Solutions were prepared using sulfuric acid (0.5 M H_2SO_4) as base electrolyte, to which methanol (Merck, p.a.) was added. Electrochemical measurements were performed with an Autolab PGSTAT302 (Ecochemie).

The formic acid oxidation was also investigated in a two-compartment cell fitted with a Pt wire and an Ag/AgCl electrode, as counter and reference electrodes, respectively. For consistency, all potentials in this work are quoted versus the RHE electrode. Working electrodes were prepared depositing a thin layer of the electrocatalyst ink over a glassy carbon disk (0.20 cm^2). Catalyst inks were prepared by mixing 2 mg of each catalyst and 15 µl of Nafion dispersion (10 wt.%, Aldrich) in 500 µl of ultrapure water (Millipore Milli-Q system). A 20 µl aliquot of the suspension was deposited onto the glassy carbon electrode and dried.

3. RESULTS AND DISCUSSION

3.1. Structural characterization of the electrocatalysts. SEM micrographs of the Pt catalysts supported on diamond powders and of the Pt/E-Tek are contrasted in **figure 1**. The faceted topography of the highly crystalline high-pressure-high-temperature diamond powders is clearly seen on **Figure 1a**. This image, taken on a Pt/ODP sample, is representative of all of the catalysts prepared, independently of the diamond surface termination. On the other hand, the SEM image of the Pt/E-Tek catalyst in **figure 1c** is characterized by aggregates of spherical carbon particles. In both cases, the topographic features are entirely dominated by the structure of the carbon grains as the Pt nanostructures are two orders of magnitude smaller.

The distribution of the Pt nanostructures can be visualized by elemental mapping, as exemplified in **figures 1b** and **1d**. Whereas it is clear that the metal is homogeneously dispersed in the case of the commercial catalyst, some aggregates can be observed when ODP is used as support material. A similar distribution was observed for Pt particles supported on HDP. Considering that the porosity of the diamond powders is very low in comparison with carbon black, it is expected that the distribution of the Pt nanostructures will be more homogeneous in the latter case.

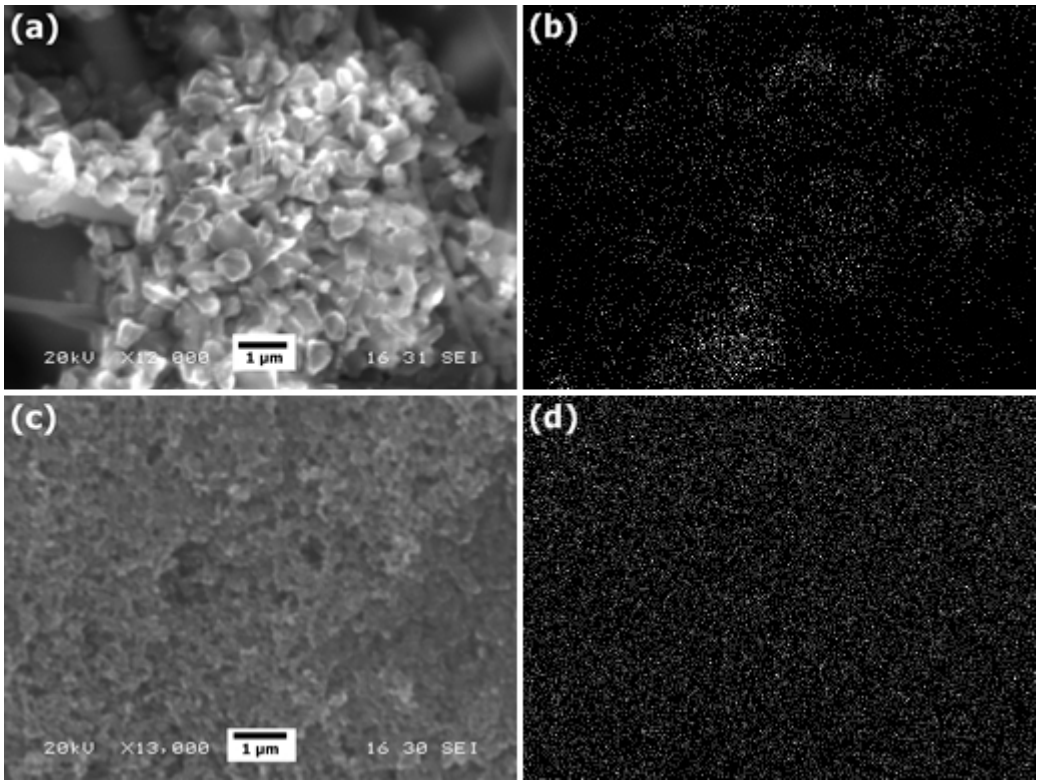

Figure 1. SEM images of Pt/ODP (a) and Pt/E-Tek (c) electrocatalysts. Corresponding Pt elemental mapping is shown as white spots for Pt/ODP and Pt/E-Tek (b and d, respectively). The scale bar in all images corresponds to 1 μm.

XRD patterns obtained for the various supported Pt nanostructures are displayed in **figure 2**. The peaks at 2θ = 40º, 47º, 67º, 81º and 85º are associated with diffraction at the (111), (200), (220), (311) and (222) planes of fcc Pt, respectively. The XRD pattern of Pt/E-Tek also displays a peak at 2θ = 26.2º, characteristic of the (002) plane of graphite. On the other hand, Pt/HDP and Pt/ODP

feature peaks at 2θ = 43.3, 74.7 and 91º, characteristic of the highly crystalline diamond particles (labeled *).[27]

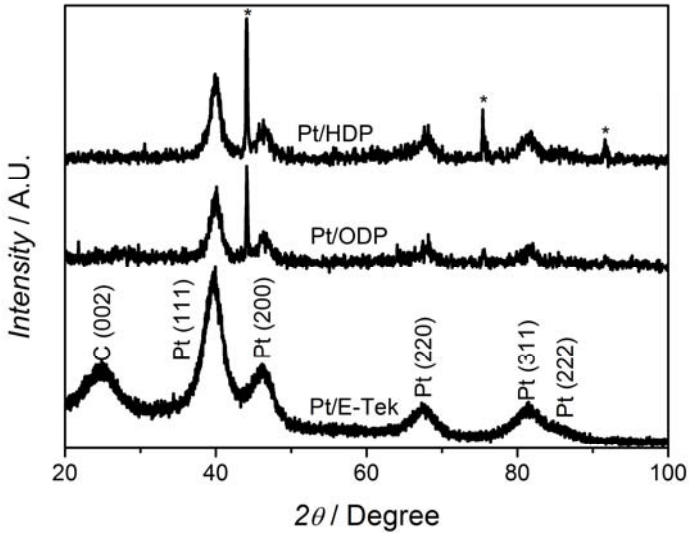

Figure 2. Powder XRD patterns of Pt/HDP, Pt/ODP and Pt/E-Tek.

Table 1 summarizes the loading and effective particle diameter (*d*) of the Pt nanostructures on the various supports as estimated from EDX and XRD data. Pt/HDP and Pt/E-Tek show similar *d* values, while the Pt particles appear somewhat larger on Pt/ODP. The overall metal loading also appears lower in the case of Pt/ODP, with respect to Pt/HDP. The difference between these two parameters in Pt/HDP and Pt/ODP is directly linked with the diamond surface termination. For instance, an increase in *d* has been reported with increasing density of surface oxygen groups in carbon black supports.[43-44] However, a unique aspect of employing diamond powder supports is that its dimensions and bulk structure are not compromised by chemical modification of the surfaces. Analysis of the XRD data allowed estimating an average lattice constant of the metal nanostructures of 3.92 Å for all samples, which is consistent with bulk Pt.

The structure and metal loading of the composites have significant effect on the electrical conductivity of the system. As described in a recent report,[34] percolation through the metal centres and "transfer doping" phenomena observed at hydrogenated surfaces are the key parameters

determining charge transport in these composites. Metal volume fractions, as estimated from the data in table 1, are just below the threshold expected for charge percolation controlled conductivity. Under these conditions, a certain proportion of metal nanoparticles appear as electrically isolated. However, as described further below, reactivity studies are normalized by the electroactive surface at each electrode. Consequently, trends in the effective reactivity of the Pt-diamond composites are less affected by the transport properties or the composite.

Table 1. Pt loading and effective particle diameter (*d*) for the various catalysts.

Electrocatalyst	% Pt	*d* / nm
Pt/HDP	14.2 ± 1.9	3.4
Pt/ODP	10.3 ± 2.2	4.8
Pt/E-Tek	16.3 ± 1.5	3.0

3.2. Oxidation of adsorbed CO. Cyclic voltammograms associated with the oxidation of adsorbed CO in 0.5 M H_2SO_4, at 5 mV s^{-1}, on all three catalysts are contrasted in **figure 3.** CO was pre-adsorbed at the electrode surface at a potential of 0.2 V, during 10 min, and argon was used for at least 20 minutes to remove CO from the electrolyte before recording the voltammograms. The first cycle is characterized by the CO_{ads} oxidation peak, which is absent in the second cycle. The appearance of the hydrogen adsorption/desorption peak at potentials lower than 0.3 V in the reverse scan and second cycle further confirm the complete oxidation of CO_{ads}. It is also observed that the voltammetric responses associated with Pt-O remain unchanged in the first and second cycle, indicating that no Pt dissolution occurs in this potential range. This set of data was employed for estimating the effective electroactive area of the Pt catalysts assuming that the charge density of

CO_{ads} under these conditions corresponds to 420 μC cm^{-2}.[45] The current responses throughout this paper were normalized to the effective surface area based on this calculation.

The commercial Pt/E-Tek catalyst features a relatively narrow CO_{ads} oxidation peak centered at 0.77 V, in contrast with the more complex responses observed for Pt/HDP and Pt/ODP. Both diamond supported Pt particles exhibited a current peak at 0.73 V, with an additional shoulder at around 0.75 V. There is no clear consensus on the origin of multiple oxidation peaks at nanostructured Pt electrodes. At well defined single crystal surfaces, oxidation peak potentials have been associated with coverage dependent adsorption energies[46] and variation in local ordering of the adlayer at different crystalographic planes[33, 47]. The shift of the CO_{ads} oxidation peak towards more negative values for the diamond supported nanoparticles with respect to Pt/E-Tek can be rationalized in terms of particle size. Several reports have suggested that the overpotential for the formation of oxygenated species at Pt nanostructures increases with decreasing particle size, which manifest itself by a shift of the CO_{ads} oxidation potential towards more positive values.[48-51] An additional aspect affecting the CO_{ads} oxidation potential is the presence of particle aggregates;[50-52] enhanced catalytic activity of Pt agglomerates has been associated with grain boundaries interconnecting nanoparticles into complex extended structures. Indeed, the 100 mV shift observed in this work is in good agreement with studies reported by Savinova and co-workers on Pt nanostructures deposited at glassy carbon electrodes.[52]

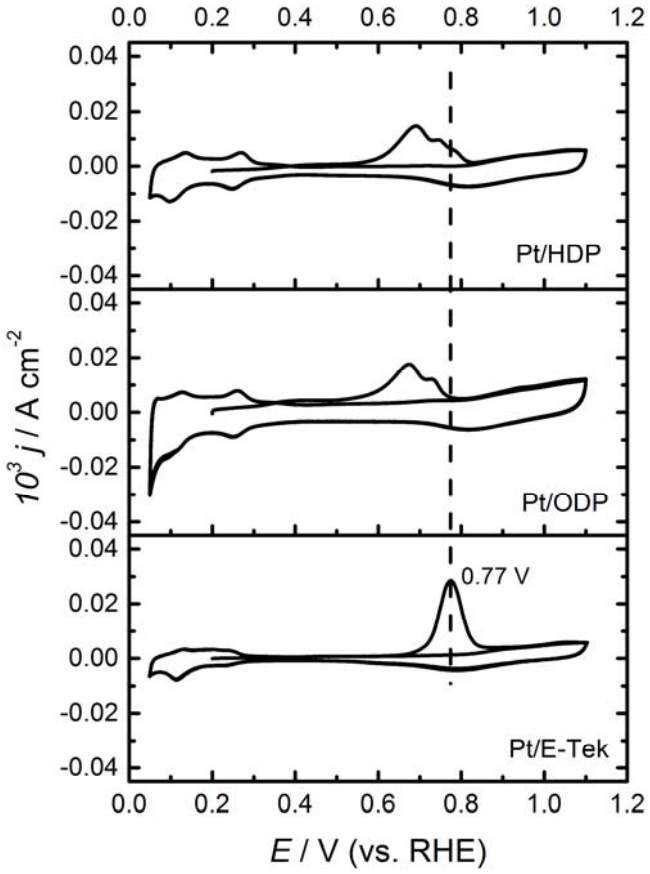

Figure 3. CO_{ads} electro-oxidation voltammograms of the different supported Pt electrocatalysts in 0.5 M H_2SO_4 at 5 mV s^{-1}. The adsorption of CO was carried out at 0.20 V and 25 ºC.

3.3. Methanol oxidation. Cyclic voltammograms associated with oxidation of methanol at the three electrocatalysts, and the corresponding DEMS signals for m/z = 44 and 60, are contrasted in **figure 4**. The experiments were carried out in electrolyte solutions containing 0.5 M methanol and 0.5 M H_2SO_4, at a scan rate of 1 mV s^{-1}. The choice of m/z values investigated is based on the volatile compounds indicated in **scheme 1**. The most effective way to monitor the generation of formic acid under the present experimental conditions is by probing m/z = 60, corresponding to methylformate, the product generated from the homogeneous reaction of formic acid and methanol. On the other hand, formaldehyde formation is significantly more challenging due to the mass overlap with methanol and the fact that these compounds do not react at low temperatures. The m/z = 44 signal is used to monitor the formation of CO_2.

The m/z = 44 ion current (middle panels) generally overlaps with the faradaic current (upper panels) in the potential scale, taking into account the time constant of the DEMS cell. In the case of m/z = 60 (lower panels in **figure 4**), there is a degree of overlap between the faradaic and mass ion currents. However, the hysteresis in the forward and reverse potential scans is significantly larger for m/z = 60 in comparison to m/z = 44. This deviation can be explained by the relatively slow ester formation (reaction between formic acid and methanol), compared to the instantaneous CO_2 formation.[53]

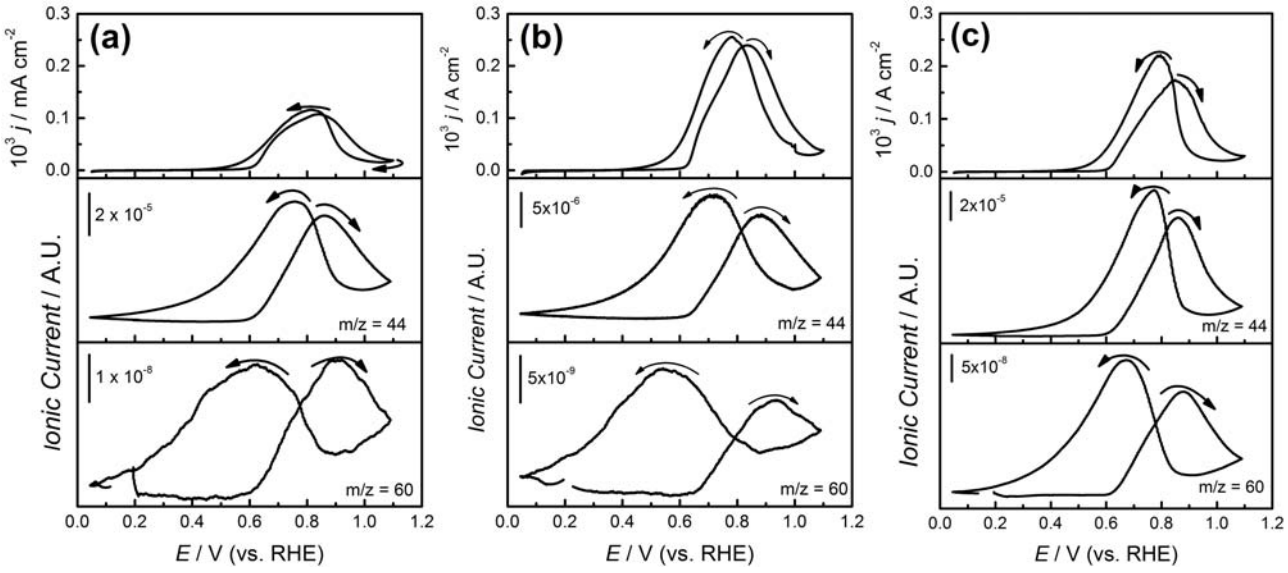

Figure 4. Cyclic voltammograms (upper panels) and DEMS signals for m/z = 44 (middle panel) and 60 (lower panels) for the oxidation of methanol (0.5 M) in 0.5 M H_2SO_4 at Pt/HDP (a), Pt/ODP (b) and Pt/C E-Tek (c) at 1 mV s^{-1}.

The results shown in **figure 5** allow a comparison between the measured faradaic current, associated with methanol oxidation, and the theoretical value estimated from the ionic current associated with CO_2 generation (m/z = 44). To perform this calculation, the CO_2 mass calibration constant (k) was estimated from DEMS measurements of CO_{ads} oxidation.[54] The difference between the measured (solid line) and estimated current (dashed line) in **figure 5** can be rationalized in terms of the formation of by-products during methanol oxidation. **Figure 5** also

shows the average faradaic efficiency calculated from the ratio of experimental and estimated charges. The data show high CO_2 conversion efficiencies for Pt/ODP and Pt/E-Tek; interestingly, Pt/HDP exhibits a lower CO_2 conversion efficiency (just below 90%). This can be associated to a higher formation of by-products (*e.g.* formic acid and formaldehyde), which are not further oxidized in the time-scale of the cyclic voltammogram.

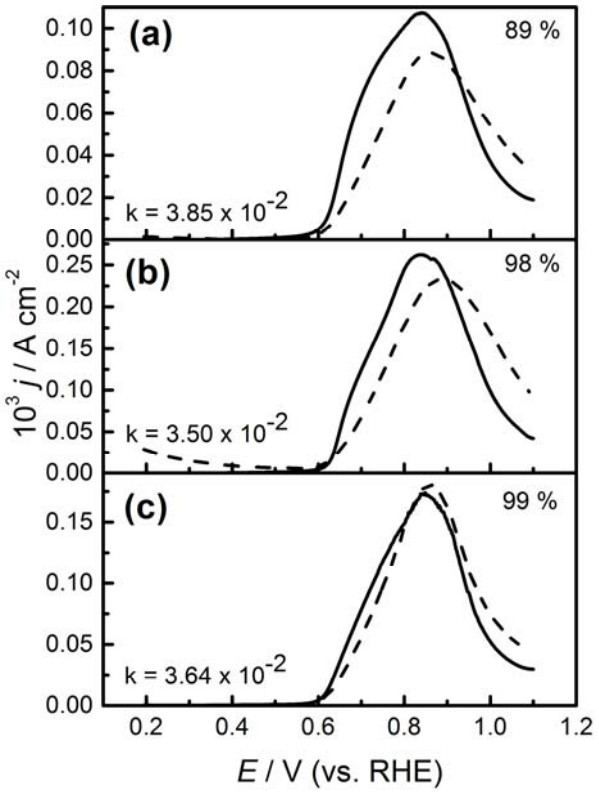

Figure 5. Experimental (——) and estimated (-- -- --) faradaic current obtained from m/z = 44 ionic currents at Pt/HDP (a), Pt/ODP (b) and Pt/E-Tek (c). Experimental conditions as in **figure 4**. The CO_2 mass calibration constant (k) used for estimation of the faradaic current from the CO_2 mass intensity is also indicated for each of the catalyst (see text).

As shown in the **supporting information**, chronoamperometric measurements recorded under similar conditions, at 0.60 V for 800 s, also show the same qualitative trend as the previous potentiodynamic experiments, i.e. lower faradaic current density for Pt/HDP in comparison to

Pt/ODP and Pt/E-Tek electrodes. Considering the systematic analysis of the experimental data, in particular the normalization of the current densities, this experimental trend cannot be simply rationalized in terms of effective surface area of the Pt catalyst. Consequently, the lower faradaic current density observed for Pt/HDP, with respect to the other catalysts, represents a so-called substrate effect associated with the hydrogenated diamond surface. Considering that the reactivity of CO_{ads} is rather similar at Pt/HDP and Pt/ODP (**figure 3**), it could be argued that the hydrogen termination does not affect this reaction pathway. On the other hand, the generation of dimethylformate as detected by DEMS data (**figure 4**) suggests that formic acid is generated as an intermediate species in methanol oxidation on all of the catalysts studied. In the final part of this work, we investigate whether a contrast in reactivity for the oxidation of formic acid in solution is observed for this family of electrocatalysts.

3.4. Formic acid oxidation. Linear sweep voltammetric data for all three catalysts, at 0.02 V s^{-1} in an electrolyte solution containing 2 M formic acid and 0.5 M H_2SO_4, are shown in **figure 6**. The onset for formic acid oxidation occurs at ca. 0.20 V, reaching a plateau between 0.55 and 0.80 V. At potentials more positive than 0.80 V, the current significantly increases with a peak emerging at 0.95 V. In the potential range below 0.80 V, Pt/HDP and Pt/ODP exhibit lower current densities than Pt/E-Tek. At potential above 0.80 V, Pt/HDP shows significantly lower current densities than both Pt/E-Tek and Pt/ODP.

It has been proposed that the voltammetric responses centered at 0.55 V correspond to the dehydrogenation of formic acid, generating CO_{ads}, while the signal at 0.95 V is attributed to the oxidative removal of CO_{ads}, along with further formic acid oxidation on 'free sites'.[55-58] On the other hand, recent studies by Cuesta and co-workers have concluded that the first step is the formation adsorbed formate , which leads to the formation of either CO_{ads} or CO_2, as illustrated in **scheme 2**.[59-61] We have already concluded that there is little reactivity contrast between Pt/HDP and Pt/ODP towards the oxidation of CO_{ads} (see **figure 3**), consequently, the apparent lower reactivity of HDP supported nanoparticles is most likely linked to the oxidation rate of $HCOO_{ads}$. Furthermore, the fact

that a significant difference is observed between Pt/ODP and Pt/E-Tek towards the oxidation of CO_{ads}, but rather little towards methanol and formic acid, further supports the conclusion that CO_{ads} oxidation is not the limiting process in the oxidation of these fuels.

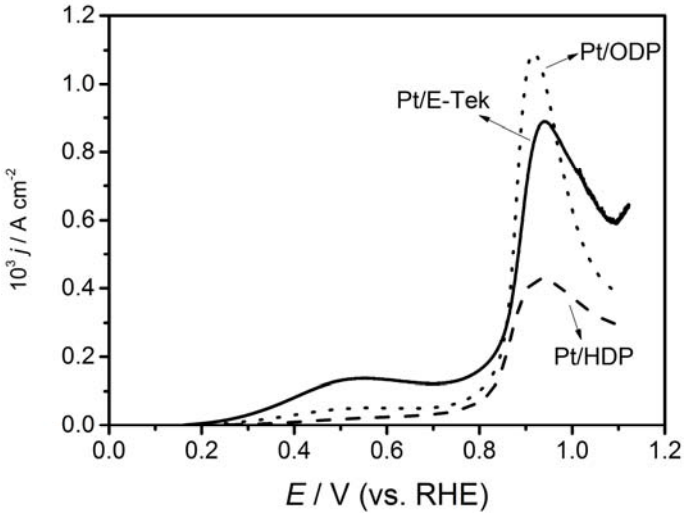

Figure 6. Linear sweep voltammetry of Pt/HDP, Pt/ODP and Pt/E-Tek in an electrolyte solution containing 2 M formic acid and 0.5 M H_2SO_4 at 0.02 V s^{-1}.

The picture emerging from these studies strongly suggests that the contrast in reactivity of Pt nanostructures supported on hydrogenated and oxygenated diamond powder towards the oxidation of formic acid and methanol is related to the oxidation rate of the $HCOO_{ads}$ species. Variations in parameters such as Pt particle size and loading, CO_{ads} oxidation potential and current density, as well as the microscopic dimensions of the diamond supports do not account for the difference observed in these studies. The key aspect which remains to be fully addressed is the link between the surface termination of the diamond support and the oxidation rate of $HCOO_{ads}$. It is well established that the hydrogenation of diamond leads to large changes in the surface dipole of up to 2.7 eV.[62-63] Hongthani et al. have recently shown that hydrogenation of identical HPHT diamond powders shifts the valance band edge energy to values close to -0.32 eV with respect to RHE.[36] We believe these electronic effects can substantially influence parameters such as the electron density at the d-band of

the metal nanoparticles, as well as the structure of water molecules around the metal centres. Both issues, which we are currently investigating, can strongly affect the binding of $HCOO_{ads}$ and the reactivity of the supported Pt nanostructures.

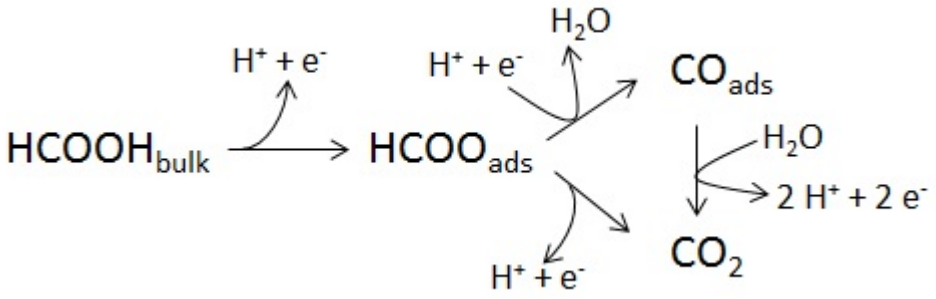

Scheme 2. Elementary steps associated with the oxidation of formic acid as suggested by Cuesta and co-workers.[61]

4. CONCLUSIONS

The electrochemical reactivity of Pt nanostructures supported on high-pressure-high-temperature diamond powders towards the oxidation of CO_{ads}, formic acid and methanol were investigated employing DEMS. The effective surface termination of the diamond powders was investigated as the key reactivity descriptor. Pt supported on hydrogen-terminated diamond powders (Pt/HDP) exhibited similar voltammetric responses for the oxidation of CO_{ads} in comparison to Pt nanostructures at oxygen-terminated powders (Pt/ODP). Both set of catalysts featured an oxidation potential for CO_{ads} over 100 mV more negative than the commercial Pt/E-Tek catalysts used as benchmark. Interestingly, a significant contrast was observed in the current density for the oxidation of methanol and formic acid on Pt/HDP and Pt/ODP. The latter showed similar behavior to Pt/E-Tek, featuring significantly high conversion efficiencies of methanol to CO_2. Pt/HDP showed methanol-to-CO_2 conversion efficiencies of 90% with smaller current densities for both methanol and formic acid. All catalysts showed evidence of formic acid formation as intermediate in methanol oxidation. The experimental evidence points towards $HCOO_{ads}$ as the key intermediate limiting the oxidation of both formic acid and methanol.

These reactivity trends, reported for the first time, are linked to the large changes in surface dipole at diamond surfaces, introducing large shifts in the relative position of the electronic bands. We expect that relatively minor effects would be observed on conducting boron-doped diamond surfaces, as the electronic interactions with the metal nanoparticles will be dominated by the continuum density of states associated to the dopant level. We are currently extending our investigations into the electronic structure of the electrocatalysts as a function of the diamond surface termination, as well as alternative formulations which could allow implementing these materials as catalysts in energy conversion systems.

ASSOCIATED CONTENT

Supporting Information

Choroamperometric transients recorded during the oxidation of methanol at the various catalysts. This material is available free of charge via the Internet at http://pubs.acs.org."

AUTHOR INFORMATION

Corresponding Authors

*E-mail: David.Fermin@bristol.ac.uk and epastor@ull.es

ACKNOWLEDGEMENTS

DP and DJF are grateful for the financial support from the UK Engineering and Physical Science Research Council (Project EP/H046305/1) and the University of Bristol. VC, MJL, EP and JFM gratefully acknowledge financial support given by the Ministry of Economy and Competitiveness through the Projects CTQ2011-28913-C02-01 and -02. VC acknowledges the financial support by CSIC/ESF for her JAE Grant, while MGM and JFM are also grateful to the support by the Mexican National Council for Science and Technology (CONACyT) and ACIISI (Gobierno de Canarias), respectively.

References

1. Jusys, Z.; Behm, R. J., Methanol, Formaldehyde, and Formic Acid Adsorption/Oxidation on a Carbon-Supported Pt Nanoparticle Fuel Cell Catalyst: A Comparative Quantitative DEMS Study. In *Fuel Cell Catalysis*, John Wiley & Sons, Inc.: 2008; pp 411-464.
2. Wang, H.; Abruña, H., Electrocatalysis of Direct Alcohol Fuel Cells: Quantitative DEMS Studies Fuel Cells and Hydrogen Storage. Bocarsly, A.; Mingos, D. M. P., Eds. Springer Berlin / Heidelberg: 2011; Vol. 141, pp 33-83.
3. Planes, G. A.; García, G.; Pastor, E., *High performance mesoporous Pt electrode for methanol electrooxidation. A DEMS study*, *Electrochem. Commun.* **2007,** *9*, 839-844.
4. Wang, H.; Löffler, T.; Baltruschat, H., *Formation of intermediates during methanol oxidation: A quantitative DEMS study*, *J. Appl. Electrochem.* **2001,** *31*, 759-765.
5. Rabis, A.; Rodriguez, P.; Schmidt, T. J., *Electrocatalysis for Polymer Electrolyte Fuel Cells: Recent Achievements and Future Challenges*, *ACS Catalysis* **2012,** *2*, 864-890.
6. Wang, H.; Baltruschat, H., *DEMS Study on Methanol Oxidation at Poly- and Monocrystalline Platinum Electrodes: The Effect of Anion, Temperature, Surface Structure, Ru Adatom, and Potential*, *J. Phys. Chem. C* **2007,** *111*, 7038-7048.
7. Jusys, Z.; Behm, R. J., *Methanol Oxidation on a Carbon-Supported Pt Fuel Cell CatalystA Kinetic and Mechanistic Study by Differential Electrochemical Mass Spectrometry*, *J. Phys. Chem. B* **2001,** *105*, 10874-10883.
8. Lázaro, M. J.; Celorrio, V.; Calvillo, L.; Pastor, E.; Moliner, R., *Influence of the synthesis method on the properties of Pt catalysts supported on carbon nanocoils for ethanol oxidation*, *J. Power Sources* **2011,** *196*, 4236-4241.
9. Calvillo, L.; Celorrio, V.; Moliner, R.; Lázaro, M. J., *Influence of the support on the physicochemical properties of Pt electrocatalysts: Comparison of catalysts supported on different carbon materials*, *Mater. Chem. Phys.* **2011,** *127*, 335-341.
10. Aksoylu, A. E.; Madalena, M.; Freitas, A.; Pereira, M. F. R.; Figueiredo, J. L., *The effects of different activated carbon supports and support modifications on the properties of Pt/AC catalysts*, *Carbon* **2001,** *39*, 175-185.
11. Sharma, S.; Pollet, B. G., *Support materials for PEMFC and DMFC electrocatalysts—A review*, *J. Power Sources* **2012,** *208*, 96-119.
12. Kim, M.; Park, J.-N.; Kim, H.; Song, S.; Lee, W.-H., *The preparation of Pt/C catalysts using various carbon materials for the cathode of PEMFC*, *J. Power Sources* **2006,** *163*, 93-97.
13. Yu, X.; Ye, S., *Recent advances in activity and durability enhancement of Pt/C catalytic cathode in PEMFC: Part I. Physico-chemical and electronic interaction between Pt and carbon support, and activity enhancement of Pt/C catalyst*, *J. Power Sources* **2007,** *172*, 133-144.
14. Calvillo, L.; Lázaro, M. J.; García-Bordejé, E.; Moliner, R.; Cabot, P. L.; Esparbé, I.; Pastor, E.; Quintana, J. J., *Platinum supported on functionalized ordered mesoporous carbon as electrocatalyst for direct methanol fuel cells*, *J. Power Sources* **2007,** *169*, 59-64.
15. Calvillo, L.; zaro, M. J.; Suelves, I.; Echegoyen, Y.; Bordej; G., E.; Moliner, R., *Study of the Surface Chemistry of Modified Carbon Nanofibers by Oxidation Treatments in Liquid Phase*, *J. Nanosci. Nanotechno.* **2009,** *9*, 4164-4169.
16. Moreno-Castilla, C.; Ferro-Garcia, M. A.; Joly, J. P.; Bautista-Toledo, I.; Carrasco-Marin, F.; Rivera-Utrilla, J., *Activated Carbon Surface Modifications by Nitric Acid, Hydrogen Peroxide, and Ammonium Peroxydisulfate Treatments*, *Langmuir* **1995,** *11*, 4386-4392.
17. Figueiredo, J. L.; Pereira, M. F. R., *The role of surface chemistry in catalysis with carbons*, *Catal. Today* **2010,** *150*, 2-7.
18. Noh, J. S.; Schwarz, J. A., *Effect of HNO3 treatment on the surface acidity of activated carbons*, *Carbon* **1990,** *28*, 675-682.
19. Darmstadt, H.; Roy, C.; Kaliaguine, S.; Choi, S. J.; Ryoo, R., *Surface chemistry of ordered mesoporous carbons*, *Carbon* **2002,** *40*, 2673-2683.

20. Celorrio, V.; Montes de Oca, M. G.; Plana, D.; Moliner, R.; Fermín, D. J.; Lázaro, M. J., *Electrochemical performance of Pd and Au–Pd core–shell nanoparticles on surface tailored carbon black as catalyst support*, *Int. J. Hydrogen Energy* **2012,** *37*, 7152-7160.
21. Materlik, G., *Diamond will shine brightly for chemistry*, *Chem. Commun.* **2003,** *0*, 1021-1023.
22. Krueger, A., *Diamond Nanoparticles: Jewels for Chemistry and Physics*, *Adv. Mater.* **2008,** *20*, 2445-2449.
23. Huang, H.; Dai, L.; Wang, D. H.; Tan, L.-S.; Osawa, E., *Large-scale self-assembly of dispersed nanodiamonds*, *J. Mater. Chem.* **2008,** *18*, 1347-1352.
24. Chakrapani, V.; Angus, J. C.; Anderson, A. B.; Wolter, S. D.; Stoner, B. R.; Sumanasekera, G. U., *Charge Transfer Equilibria Between Diamond and an Aqueous Oxygen Electrochemical Redox Couple*, *Science* **2007,** *318*, 1424-1430.
25. Liu, Y.; Gu, Z.; Margrave, J. L.; Khabashesku, V. N., *Functionalization of Nanoscale Diamond Powder: Fluoro-, Alkyl-, Amino-, and Amino Acid-Nanodiamond Derivatives*, *Chem. Mater.* **2004,** *16*, 3924-3930.
26. Krueger, A.; Lang, D., *Functionality is Key: Recent Progress in the Surface Modification of Nanodiamond*, *Adv. Funct. Mater.* **2012,** *22*, 890-906.
27. Moore, A.; Celorrio, V.; de Oca, M. M.; Plana, D.; Hongthani, W.; Lazaro, M. J.; Fermin, D. J., *Insulating diamond particles as substrate for Pd electrocatalysts*, *Chem. Commun.* **2011,** *47*, 7656-7658.
28. Wang, J.; Swain, G. M., *Fabrication and Evaluation of Platinum/Diamond Composite Electrodes for Electrocatalysis*, *J. Electrochem. Soc.* **2003,** *150*, E24-E32.
29. Spătaru, N.; Zhang, X.; Spătaru, T. a.; Tryk, D. A.; Fujishima, A., *Platinum Electrodeposition on Conductive Diamond Powder and Its Application to Methanol Oxidation in Acidic Media*, *J. Electrochem. Soc.* **2008,** *155*, B264.
30. Spătaru, T.; Anastasescu, M.; Spătaru, N.; Fujishima, A., *Influence of cobalt oxide substrate on the resistance to fouling during methanol oxidation of platinum particles*, *Electrochem. Commun.* **2013,** *29*, 1-3.
31. La-Torre-Riveros, L.; Abel-Tatis, E.; Méndez-Torres, A.; Tryk, D.; Prelas, M.; Cabrera, C., *Synthesis of platinum and platinum–ruthenium-modified diamond nanoparticles*, *J. Nanopart. Res.* **2011,** *13*, 2997-3009.
32. La-Torre-Riveros, L.; Guzman-Blas, R.; Méndez-Torres, A. E.; Prelas, M.; Tryk, D. A.; Cabrera, C. R., *Diamond Nanoparticles as a Support for Pt and PtRu Catalysts for Direct Methanol Fuel Cells*, *ACS Appl. Mater. Interfaces* **2012,** *4*, 1134-1147.
33. López-Cudero, A.; Solla-Gullón, J.; Herrero, E.; Aldaz, A.; Feliu, J. M., *CO electrooxidation on carbon supported platinum nanoparticles: Effect of aggregation*, *J. Electroanal. Chem.* **2010,** *644*, 117-126.
34. Plana, D.; Humphrey, J. J. L.; Bradley, K. A.; Celorrio, V.; Fermín, D. J., *Charge Transport Across High Surface Area Metal/Diamond Nanostructured Composites*, *ACS Appl. Mater. Interfaces* **2013,** *5*, 2985-2990.
35. Maier, F.; Riedel, M.; Mantel, B.; Ristein, J.; Ley, L., *Origin of Surface Conductivity in Diamond*, *Phys. Rev. Lett.* **2000,** *85*, 3472-3475.
36. Hongthani, W.; Fox, N. A.; Fermín, D. J., *Electrochemical Properties of Two Dimensional Assemblies of Insulating Diamond Particles*, *Langmuir* **2011,** *27*, 5112-5118.
37. Plana, D.; Humphrey, J. J. L.; Bradley, K. A.; Celorrio, V.; Fermín, D. J., *Charge Transport Across High Surface Area Metal/Diamond Nanostructured Composites*, *ACS Applied Materials & Interfaces* **2013,** *DOI: 10.1021/am302397p*.
38. Holt, K. B., *Undoped diamond nanoparticles: origins of surface redox chemistry*, *PCCP* **2010,** *12*, 2048-2058.
39. Hongthani, W.; Fermín, D. J., *Layer-by-Layer assembly and redox properties of undoped HPHT diamond particles*, *Diamond Relat. Mater.* **2010,** *19*, 680-684.
40. Holt, K. B.; Ziegler, C.; Zang, J.; Hu, J.; Foord, J. S., *Scanning Electrochemical Microscopy Studies of Redox Processes at Undoped Nanodiamond Surfaces*, *J. Phys. Chem. C* **2009,** *113*, 2761-2770.
41. Pérez-Rodríguez, S.; Corengia, M.; García, G.; Zinola, C. F.; Lázaro, M. J.; Pastor, E., *Gas diffusion electrodes for methanol electrooxidation studied by a new DEMS configuration: Influence of the diffusion layer*, *Int. J. Hydrogen Energ.* **2012,** *37*, 7141-7151.
42. Pérez-Rodríguez, S.; García, G.; Calvillo, L.; Celorrio, V.; Pastor, E.; Lázaro, M. J., *Carbon-Supported Fe Catalysts for CO2 Electroreduction to High-Added Value Products: A DEMS Study: Effect of the Functionalization of the Support*, *Int. J. Electrochem.* **2011,** *2011*, DOI: 10.4061/2011/249804.

43. Fraga, M. A.; Jordão, E.; Mendes, M. J.; Freitas, M. M. A.; Faria, J. L.; Figueiredo, J. L., *Properties of Carbon-Supported Platinum Catalysts: Role of Carbon Surface Sites*, *J. Catal.* **2002,** *209*, 355-364.
44. Guerrero-Ruiz, A.; Badenes, P.; Rodríguez-Ramos, I., *Study of some factors affecting the Ru and Pt dispersions over high surface area graphite-supported catalysts*, *App. Catal. A-General* **1998,** *173*, 313-321.
45. Vidaković, T.; Christov, M.; Sundmacher, K., *The use of CO stripping for in situ fuel cell catalyst characterization*, *Electrochim. Acta* **2007,** *52*, 5606-5613.
46. Marković, N. M.; Ross Jr, P. N., *Surface science studies of model fuel cell electrocatalysts*, *Surface Science Reports* **2002,** *45*, 117-229.
47. Solla-Gullón, J.; Vidal-Iglesias, F. J.; Herrero, E.; Feliu, J. M.; Aldaz, A., *CO monolayer oxidation on semi-spherical and preferentially oriented (1 0 0) and (1 1 1) platinum nanoparticles*, *Electrochem. Commun.* **2006,** *8*, 189-194.
48. Maillard, F.; Eikerling, M.; Cherstiouk, O. V.; Schreier, S.; Savinova, E.; Stimming, U., *Size effects on reactivity of Pt nanoparticles in CO monolayer oxidation: The role of surface mobility*, *Faraday Discuss.* **2004,** *125*, 357-377.
49. Hayden, B. E.; Pletcher, D.; Suchsland, J.-P.; Williams, L. J., *The influence of support and particle size on the platinum catalysed oxygen reduction reaction*, *PCCP* **2009,** *11*, 9141-9148.
50. Wang, S.; Jiang, S. P.; White, T. J.; Guo, J.; Wang, X., *Electrocatalytic Activity and Interconnectivity of Pt Nanoparticles on Multiwalled Carbon Nanotubes for Fuel Cells*, *J. Phys. Chem. C* **2009,** *113*, 18935-18945.
51. Cherstiouk, O. V.; Simonov, P. A.; Savinova, E. R., *Model approach to evaluate particle size effects in electrocatalysis: preparation and properties of Pt nanoparticles supported on GC and HOPG*, *Electrochim. Acta* **2003,** *48*, 3851-3860.
52. Maillard, F.; Schreier, S.; Hanzlik, M.; Savinova, E. R.; Weinkauf, S.; Stimming, U., *Influence of particle agglomeration on the catalytic activity of carbon-supported Pt nanoparticles in CO monolayer oxidation*, *PCCP* **2005,** *7*, 385-393.
53. Jusys, Z.; Kaiser, J.; Behm, R. J., *Methanol Electrooxidation over Pt/C Fuel Cell Catalysts: Dependence of Product Yields on Catalyst Loading*, *Langmuir* **2003,** *19*, 6759-6769.
54. García, G.; Florez-Montaño, J.; Hernandez-Creus, A.; Pastor, E.; Planes, G. A., *Methanol electrooxidation at mesoporous Pt and Pt–Ru electrodes: A comparative study with carbon supported materials*, *J. Power Sources* **2011,** *196*, 2979-2986.
55. Liu, Z.; Hong, L.; Tham, M. P.; Lim, T. H.; Jiang, H., *Nanostructured Pt/C and Pd/C catalysts for direct formic acid fuel cells*, *J. Power Sources* **2006,** *161*, 831-835.
56. Wu, Y. N.; Liao, S. J.; Su, Y. L.; Zeng, J. H.; Dang, D., *Enhancement of anodic oxidation of formic acid on palladium decorated Pt/C catalyst*, *J. Power Sources* **2010,** *195*, 6459-6462.
57. Hong, P.; Luo, F.; Liao, S.; Zeng, J., *Effects of Pt/C, Pd/C and PdPt/C anode catalysts on the performance and stability of air breathing direct formic acid fuel cells*, *Int. J. Hydrogen Energy* **2011,** *36*, 8518-8524.
58. Jovanović, V. M.; Tripković, D.; Tripković, A.; Kowal, A.; Stoch, J., *Oxidation of formic acid on platinum electrodeposited on polished and oxidized glassy carbon*, *Electrochem. Commun.* **2005,** *7*, 1039-1044.
59. Samjeské, G.; Miki, A.; Ye, S.; Osawa, M., *Mechanistic Study of Electrocatalytic Oxidation of Formic Acid at Platinum in Acidic Solution by Time-Resolved Surface-Enhanced Infrared Absorption Spectroscopy*, *J. Phys. Chem. B* **2006,** *110*, 16559-16566.
60. Osawa, M.; Komatsu, K.-i.; Samjeské, G.; Uchida, T.; Ikeshoji, T.; Cuesta, A.; Gutiérrez, C., *The Role of Bridge-Bonded Adsorbed Formate in the Electrocatalytic Oxidation of Formic Acid on Platinum*, *Angew. Chem. Int. Ed.* **2011,** *50*, 1159-1163.
61. Cuesta, A.; Cabello, G.; Gutierrez, C.; Osawa, M., *Adsorbed formate: the key intermediate in the oxidation of formic acid on platinum electrodes*, *PCCP* **2011,** *13*, 20091-20095.
62. Haertl, A.; Garrido, J. A.; Nowy, S.; Zimmermann, R.; Werner, C.; Horinek, D.; Netz, R.; Stutzmann, M., *The ion sensitivity of surface conductive single crystalline diamond*, *J. Am. Chem. Soc.* **2007,** *129*, 1287-1292.
63. O'Donnell, K. M.; Martin, T. L.; Fox, N. A.; Cherns, D., *Ab initio investigation of lithium on the diamond C(100) surface*, *Physical Review B* **2010,** *82*, 115303.

TOC ILLUSTRATION